Eur. Phys. J. Plus (2019) **134**: 269
DOI 10.1140/epjp/i2019-12705-0

THE EUROPEAN PHYSICAL JOURNAL PLUS

Regular Article

Material composition evaluation of historical Cu alloy aquamanilia by complementary XRF and LIBS measurements[⋆] [⋆⋆]

I. Żmuda-Trzebiatowska[1], J.M. del Hoyo-Meléndez[2,a], and G. Śliwiński[1]

[1] Department of Photophysics, The Szewalski Institute IF-FM, Polish Academy of Sciences, 14 Fiszera St, 80-231 Gdańsk, Poland
[2] Laboratory of Analysis and Non-Destructive Investigation of Heritage Objects, National Museum in Kraków, 14 Piłsudskiego St, 31-109, Kraków, Poland

Received: 24 August 2018 / Revised: 4 April 2019
Published online: 18 June 2019

Abstract. The material composition of seven historical *aquamanilia* from museum collections in Kraków and Gdańsk were examined using X-ray fluorescence (XRF) spectrometry and micro-ablation sampling by means of laser-induced breakdown spectroscopy (LIBS) to better understand the materials found in these objects as well as for providing information that can be used towards authentication and dating studies. An additional set of Cu-alloy objects and also a late medieval XV century bronze *aquamanile* served for reference and comparison. It was found that four of the figures were casted using quaternary and ternary Cu alloys characterized by a Zn content in the range 17.5–23%, admixtures of Sn and Pb below 7%, and presence of impurities like Fe, Ni, Ag, Si, Ba, and Ca. The observed composition similarities were confirmed by statistically processed data. This indicated that the animal figures (lions) are most probably brass replicas of the medieval ones and were produced during the XVIII–XX centuries. *In situ* measurements were adequate despite inaccuracies associated with signal intensity fluctuations due to surface geometry effects, the presence of patinas, corrosion or contamination, and systematic errors originating from calibration. The proposed complementary approach that uses portable XRF and LIBS instruments ensures consistent data for compositional studies on historical alloys.

1 Introduction

Investigations of cultural heritage metallic artifacts often involve analysis of the chemical composition of the materials found in the objects. The knowledge about the materials is essential for answering questions related to the object's origin and authentication, its provenance, trade routes, and to better understand the production technologies of the past [1–3]. Moreover, understanding the deterioration of materials, specifically corrosion processes of metal objects, is essential for designing conservation treatments and formulating an informed preservation plan with the aim of protecting and passing on these objects in a good state of preservation to future generations [4–6]. Due to the variety and unique character of cultural heritage objects, the research on this subject requires a multidisciplinary approach that involves experts from different areas such as physics, chemistry, conservation, art history, and archaeology, among others. Such an integrated approach ensures an effective use of appropriate analytical techniques and a high level of confidence in the obtained data, while providing valuable information for developing a preventive conservation strategy [7,8]. Previous case studies and review papers have confirmed that non-destructive analysis together with knowledge of the application range and limitations of analytical techniques are of key importance for the study of cultural heritage objects [9, 10]. Among the available analytical tools, X-ray fluorescence (XRF) spectrometry and laser-induced breakdown spectroscopy (LIBS) belong to the most preferred methods for compositional studies of historical metals and alloys [11–15]. Frahm *et al.* [16] discussed the methodological and theoretical aspects of XRF when applied to the study of historical objects. The potential of the LIBS technique has been confirmed for a variety of inorganic and organic materials, such as stone [17], metals [18], pigments [19], and paper [20]. Moreover, the important role of LIBS in the characterization

[⋆] Focus Point on "Scientific Research in Conservation Science" edited by L. Bellot-Gurlet, D. Bersani, P. Vandenabeele.
[⋆⋆] Supplementary material in the form of a .pdf file available from the Journal web page at https://doi.org/10.1140/epjp/i2019-12705-0

[a] e-mail: jdelhoyo@mnk.pl

of original materials and the detection of restoration interventions as well as its potential for provenance and dating studies have been reviewed by Spizzichino and Fantoni [21,22]. The main advantages of these two techniques are: i) high sensitivity in the range $\sim$ 1–100 ppm; ii) non-destructive testing in the case of XRF and micro-destructive analysis of LIBS, based on sampling where a few micrograms of material are evaporated; iii) immediate measurement results; and iv) capability of field applications (*in situ* analysis) by means of portable/transportable instruments.

Non-destructive methods offer the advantage of performing a non-invasive analysis, which eliminates the requirement of extracting samples from objects and do not require any sample preparation prior to performing the measurements. These methods include imaging techniques such as X-ray radiography [23] and computed tomography [24] together with physicochemical techniques such as X-ray fluorescence (XRF) spectrometry [15]. The benefit of this approach is the protection of original surfaces since after the measurements, the objects do not exhibit any visible alteration. Other analytical techniques such as laser ablation inductively coupled plasma mass spectrometry (LA-ICP-MS) [25] and secondary ion mass spectrometry (SIMS) [26] may provide accurate quantitative data, but they are considered destructive since the sample material is consumed during the analysis resulting sometimes impractical for the study of museum collections.

The interpretation of results, however, requires a different approach in both cases due to differences in the detection mechanism, spot geometry, and depth of penetration. In XRF, the thickness of the examined surface layer depends on the penetration depth of the primary X-ray beam, which for metals ranges up to about several micrometers, together with the escape depth from which fluorescent X-rays can be detected. This may cause interpretation problems if the metal surface is covered by a corrosion and/or patina layer that contributes to the spectrum. In the case of LIBS, the spectra of laser-ablated and vaporized micro-samples are acquired. The thickness of the ablated layer does not exceed 1–2 μm per laser pulse and depends on the laser energy density, the layer composition, and side effects such as self-absorption. LIBS micro-sampling repeated at the same location on the object surface results in its stepwise and controlled micro-penetration, while the subsequent spectra make it possible to conduct stratigraphic analyses of the penetration-depth-related elemental composition of the material under question [17,21,27]. The two techniques discussed above are adequate for performing materials analysis of metallic cultural heritage objects and were employed in this work for the investigation of a group of *aquamanilia*.

Aquamanilia are vessels used for pouring water during hand washing ceremonies —originally during liturgical rituals and later on during meals in the upper society echelons of the Middle Ages. Their function is adequately described by the name *aquamanile* composed from Latin words *aqua* and *manus*. Most *aquamanilia* were made of copper alloys through the lost-wax casting process. The production technology and tradition of using these hollow-cast vessels with animal forms existed in late Roman, Byzantine, and Islamic cultures and were brought to Europe by the Crusaders (1095–1204) as described by Barnet and Dandridge [28]. However, according to these authors, the available sources are insufficient to conclude on relationships between Eastern and Western objects and to answer the question whether forms of the latter ones were adopted or copied by European craftsmen. Also, this author provides estimate dating and provenance of some *aquamanilia* grouped by the characteristic figure details such as engraved patterns, masks, and surface ornaments, among others. Many surviving *aquamanilia* were created between 1200 and 1450 in Germany, in regions with a renowned metalwork tradition, initially in Magdeburg and Hildesheim and later on in Nuremberg, towards the end of the cited period.

Aquamanilia are scarce in museum collections. The uniqueness and design of the finely crafted "functionalized" figures were probably the reasons why *aquamanilia* often have been copied in various sizes during the XIXth and XXth centuries [28–30] resulting in recent authentication problems. The impressive animal-shaped figures (lions, dogs, dragons, griffins, etc.) can be admired mostly as singular specimens in museums around the world including the Rijksmuseum in Amsterdam, the Metropolitan Museum of Art in New York (one of the largest collections), the National Gallery of Art in Washington, and the Germanisches Nationalmuseum in Nuremberg.

This paper presents a methodology for the complementary use of XRF and LIBS for studying the alloy composition of a group of historical *aquamanilia*. The materials composition of the objects belonging to collections of the National Museum in Kraków and Gdańsk was analyzed to provide reliable data that can be used towards the development of informed conservation treatments and for authentication and dating studies. First, qualitative XRF measurements provided the elemental composition of the objects followed by an evaluation of the results, which allowed to determine their material composition quantitatively. To confirm the composition differences, the LIBS sampling was carried out on selected areas of the objects. The results of the complementary measurements were evaluated statistically and compared with those obtained for a group of historical objects belonging to a reference collection. The results permitted to assess the material composition, to identify the sources of errors, and to test the reliability of the proposed complementary approach.

2 Objects

The group of investigated *aquamanilia* is shown in fig. 1. In the selection of reference for objects A, C, D, and F, in particular, the literature data on metallic historical vessels in the form of lions were taken into account. According to Barnet

Fig. 1. *Aquamanilia* studied in this work: objects marked as A and G and C, D, E, F belong to the collections of the National Museums in Gdańsk and Kraków. Object B belongs to the Germanisches Nationalmuseum in Nuremberg, catalogue No. KG261. The black dots show the approximate locations of the measurements.

and Dandridge [28], this form characterizes about 1/3 of the surviving objects, which differ in dimensions, ornamentation, details and material composition (bronze, brass). *Aquamanile* B was chosen as a reference due to its similarity in form and appearance. This object was donated around 1852 by the Nuremberg Museum founder, H. v. Aufsess. The material composition and information on production period were obtained from XRF measurements and historical studies, respectively [29–31], and agree with data provided by the museum (`http://objektkatalog.gnm.de/objekt/KG261`). A brief description of the investigated objects is provided in table 1.

The animal figures are characterized by a hollow body, which can be filled with water through an opening in their heads. For hand washing, the water flows out through the opening in the mouth, while the long double-curved tail serves as a handle [15,28–30]. *Aquamanile* A is characterized by a short cylindrical pipe in the mouth opening, a miniature lion mask with the initials P, S, datum "1744" stamped on the lion's chest, and local discoloration of the body surface (see inset in fig. 1). The incomplete object D represents a cross-section of the lion's body made vertically through the head and horizontally through the chest. It measures about 8 cm in height indicating that the original dimensions might be very similar to those of objects A and C. *Aquamanile* E is the largest evaluated object (height 47.7 cm, diameter 15.8 cm) in the present study, while G is the smallest one and has the form of a flying dragon ($11.7 \times 9.8 \times 5.7$ cm). The latter was a gift to the museum from a fisherman who found the object in the Baltic Sea in 2007. Photographs made prior and after restoration indicate the difference between the heavily corroded and the remaining discolored surface areas with perforations.

Table 1. Description of the evaluated *aquamanilia*.

Object ID	Figure form	Date	Institution	Inventory number
A	Lion	XIX century	NMG	MNG/SD/590/Mt
B	Lion	XV century	GNMN	KG261
C	Lion	1850–1900	NMK	MNK IV-M-2845
D	Lion fragment	XX century	NMK	MNK IV-M-1945
E	Large jug with dog	End of XV century	NMK	MNK IV-M-458
F	Lion	XIX century	NMK	MNK IV-M-3121
G	Flying dragon	XIX century	NMMG	CMM/SM/3740

It is worth to notice that conservators involved in the current study indicated the difficulty of identifying the interface between surface layers of unwanted matter and original material. The corrosion typically produces inhomogeneous layers of various thicknesses where boundaries are difficult to locate. Therefore, it is problematic to remove unwanted matter without removing original material caught up in the degraded layers above, within, or below the original surface. Active corrosion, characterized by the development of a light green powder erupting in spots over the surface, was found at the surface of aquamanile G. This powdery green corrosion is usually removed mechanically. The conservation treatment involved polishing the object in order to recover its original appearance using an abrasive paste consisting of precipitated calcium carbonate ($CaCO_3$) in combination with water using cotton pads or cloths. Next, the object was cleaned with wet rags to remove the polishing paste and a micro-crystalline wax coating was applied to provide protection against both the environmental factors and handling.

The small size of object G in relationship with other objects in fig. 1 becomes evident when putting this object in context with *aquamanilia* from other collections, *e.g.*, the Metropolitan Museum (New York) where some of the objects are characterized by height and mass up to about 40 cm and 6 kg, respectively [32].

3 Experimental section

Preliminary measurements of the material composition of *aquamanilia* were performed with the use of two XRF spectrometers, designated as XRF_I (Pomerania Lab, Gdańsk) and XRF_{II} (LANBOZ, Kraków). XRF_I (IF-FM brand) used for measurements conducted on objects A and G is equipped with a tungsten X-ray tube (IS601.5, Italstructures) operated at 45 kV and 1 mA, and a collimated beam producing a spot of about 2 mm in diameter. The energy resolution of the SDD detector (AXAS, Ketek) was 155 eV (Mn K_α line, 5.9 keV) and the detection limits (Cu matrix, single standard method, 95% confidence level) were 0.005% for Cu and 0.04% for Pb and Sn.

XRF_{II} was used for measurements on objects C, D, E and F. The Artax 400 spectrometer (Bruker) is equipped with a Rh X-ray tube operated at 40 kV and 0.995 mA. Depending on the areas investigated for a particular object, two collimators resulting in beam spot sizes of 0.65 and 1.5 mm were employed. The Artax software (Spectra 5.3, Bruker) was used for qualitative analysis of the spectra.

For consistency, instruments XRF_I and XRF_{II} were calibrated with the set of Cu-alloy standards described above —see table S1 in the electronic supplementary material (ESM). The accumulation time employed was 120 s. Due to observed scattering of the measurement data associated with surface effects, the presence of corrosion and surface contamination, the material composition was obtained from spectra averaged over at least 5 accumulations.

In addition, the handheld spectrometer XRF_T —S1 Titan LE (Bruker)— equipped with a Rh tube and X-Flash® SDD detector, was employed to carry out an initial screening of the objects. The XRF_T (spot size 5 mm) was operated at 50 kV and 15 μA, and the acquisition time employed was 30 s. This instrument allowed performing preliminary quantitative analyses of the *aquamanilia* since it has several internal calibrations for metal alloys that are based on the fundamental parameter (FP) method. The S1 RemoteCtrl and the S1 Sync software were employed for instrument control, while the Artax software was also used for spectral analysis.

LIB spectra were acquired by means of a transportable instrument AvaLIBS (Avantes) under pulsed excitation provided by the laser Ultra UL130 (Quantel) operated at 1064 nm with a constant pulse energy of 50 mJ, a pulse duration of 7 ns and at fluence not exceeding 2 J/cm^2. Spectra were acquired using a multichannel spectrometer equipped with gratings of 2400, 1800 and 1200 groves/mm and coupled with a CCD camera both controlled by the Avasoft and Avaspec packages. Measurements were performed in the spectral range 200–900 nm with a resolution not lower than 0.1 nm using fixed integration time and delay of 2 μs. The laser spot size at the sample surface was about 150 μm and the LIB spectra were obtained as averages of at least ten measurements on the same location. Measurements were performed exclusively on unexposed surface areas as required by the museum curators.

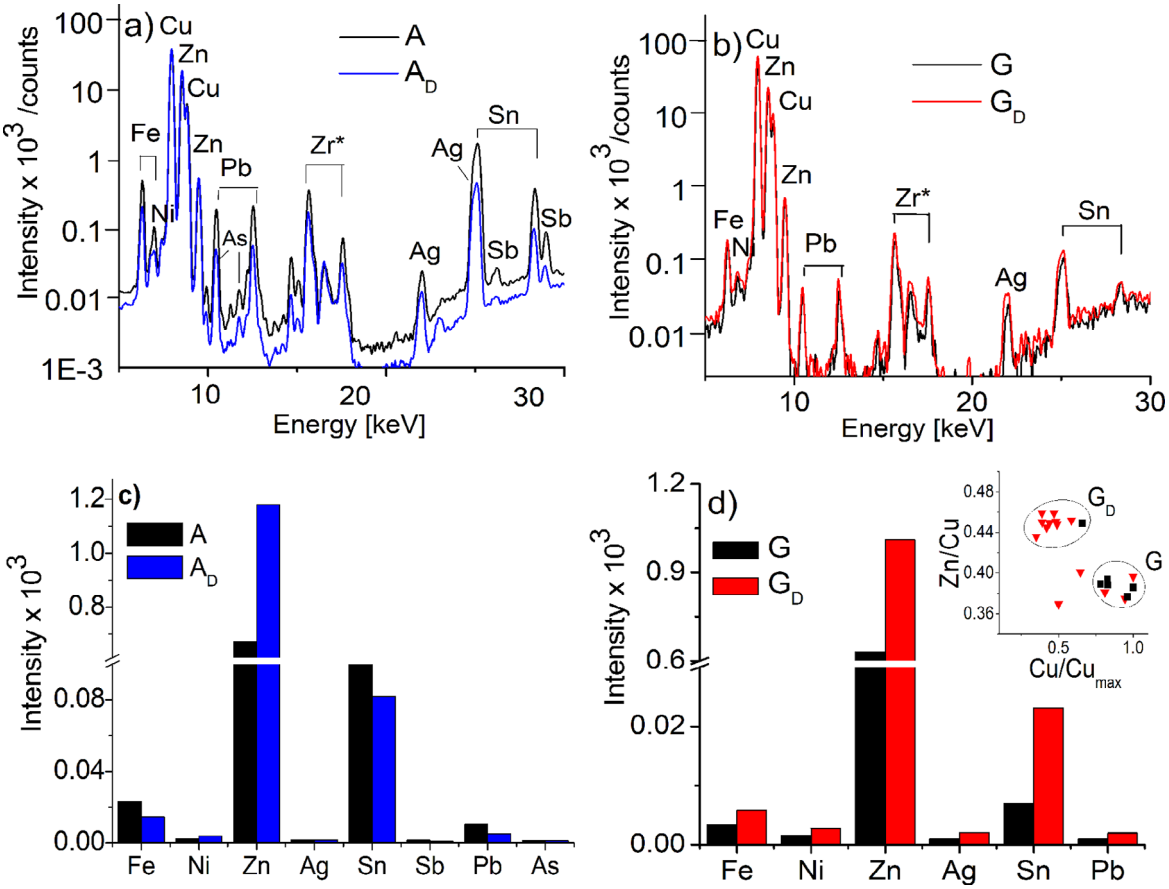

Fig. 2. Summary of XRF results. (a) Spectra registered for object A. (b) Spectra registered for object G. Comparison of net peak areas of main elements (without Cu) of object A, A_D (c) and G, G_D (d). Inset in (d) shows the Zn/Cu ratios *versus* relative Cu content measured for various surface spots of G and G_D. Original and defect areas are indicated by the object's letter and the object's letter with the subscript D, respectively. Black and color XRF spectra are used to differentiate original and defect areas, respectively.

Quantitative analysis of the alloys was conducted using the three instruments described above: XRF_I, XRF_{II}, and LIBS. For this purpose, an empirical calibration was performed for instruments XRF_I and XRF_{II} using the same set of Cu-alloy standards certified by the Institute of Non-Ferrous Metals (Gliwice, PL). Calibration curves were obtained by plotting the net peak areas calculated for the main elements observed in the spectra of the multi-element standards *versus* the elemental concentrations (% wt) reported by the manufacturer. The method was validated by treating two of the standards in the set as unknown samples (in a preliminary calibration) and by comparing the values obtained from the empirical calibration with the percentages reported by the XRF_T, which were obtained using the FP method. The relative standard deviations (RSD_m) of the measured and nominal contents were used to estimate the uncertainty of the quantification method. As discussed by Mass and Shugar [15], this calibration approach was necessary in view of the proper validation and comparison of the quantitative data obtained using different instruments.

4 Results and discussion

4.1 Alloy compositions

Averaged XRF spectra of *aquamanila* were obtained from a series of measurements made at different locations, which are shown in fig. 1. For object G, data were collected after removal of the corrosion layer and surface cleaning, but before application of the protective coating. For objects A (lion) and G (dragon), revealing locally discolored areas, XRF spectra designated as A_D and G_D were collected and are summarized in fig. 2(a), (b). The dominating bands ascribed to Cu, Zn, Sn, and Pb indicate the use of a quaternary copper alloy for both of these objects. The presence of typical admixtures is inferred from observed peaks of Ag and Ni, while the peak of Fe can be associated with the ore (chalcopyrite) used for the production of the alloy, corrosion layers and/or surface contamination (iron oxides) as previously reported [2]. Color differences between original (A) and discolored (A_D) areas were clearly discerned visually. This observation was in agreement with XRF line intensities of Pb and Sn, which were relatively higher for original

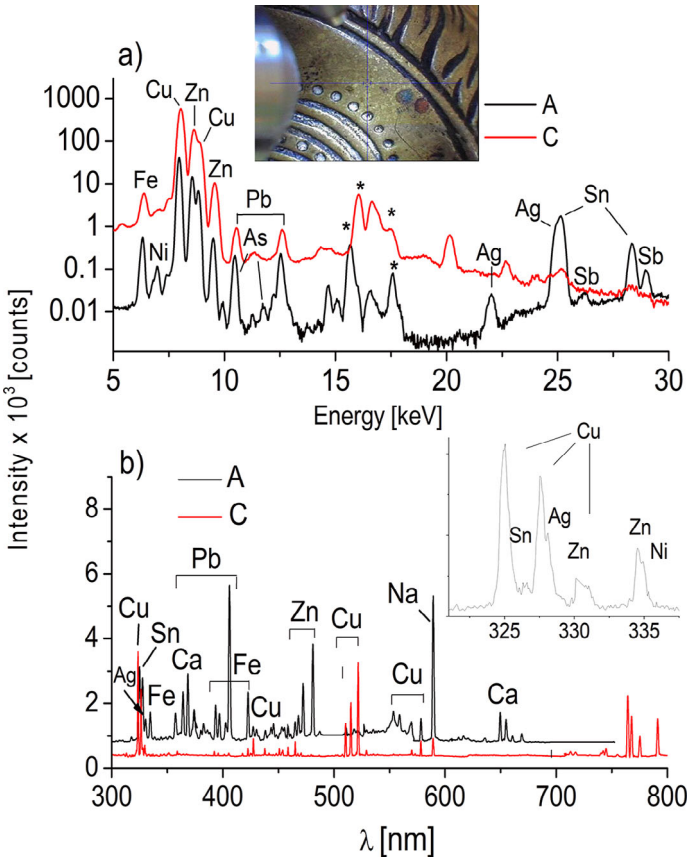

Fig. 3. Comparison of (a) XRF and (b) LIBS spectra obtained for object C on the approximate location shown in the photograph. The inset in (b) shows a detail of the LIBS spectrum of A acquired from an unexposed surface area.

areas (brighter appearance) relative to discolored ones. For object G, the discrimination between averaged spectra G and G_D is difficult due to a relatively large variation of the recorded spectral intensities (fig. 2(b)) attributable to surface effects characteristic of each tested location. Comparison of the net peak areas obtained after baseline subtraction and deconvolution of spectra lead to a similar conclusion (fig. 2(c), (d)). In the case of *aquamanile* A, different contents of the alloy components and admixtures were observed after comparing A with A_D. This is in agreement with the visible color difference and sharp interface exhibited by these two areas (see inset in fig. 1). This confirms the repair in area A_D with the use of an alloy different from the one used for making *aquamanile* A.

The higher signal intensity observed for all detected elements in area G_D (fig. 2(d)) can be explained after considering the elemental contents from the non-averaged spectra. The Zn/Cu intensity ratios plotted as a function of the Cu intensity measured for different locations clearly show two material groups (see inset in fig. 2(d)). This observation coincides with the visually observed differences between zones G and G_D. The scattering of the data is not surprising if one takes into account the long-term exposure of G to a corrosive seawater environment. This resulted in the observed inhomogeneity of material composition, surface perforations, and variations in color from reddish to grayish-green to grey, and the partially darkened areas of the region G_D. The relatively lower content of Zn in G_D and differences in relative Cu intensities can be in part due to the presence of corrosion products at the surface layer. Dezincification in saline environments is typical for alloys containing a substantial amount of Zn, which is a particularly susceptible element to de-alloying via parting corrosion [33–35]. In this process, Zn corrodes selectively and leaves a porous copper matrix that maintains its shape but has little mechanical strength. Depending on the conditions (stagnant or turbulent seawater) the corroded layer can be superficial or penetrate deeper into the material. This layer is characterized by corrosion rates ranging between 0.01 and 0.025 mm/year. Moreover, it is known that the corrosion of Cu-alloys in seawater environment, results in the formation of a multicomponent corrosion coverage of the object surface with the presence of typical products such as atacamite ($Cu_2(OH)_3Cl$), chalcopyrite ($CuFeS_2$), cuprite (Cu_2O) and tenorite (CuO) [36]. Instantaneously, due to the action of sulphate reducing bacteria, an oxalate patina can be formed, which has been well documented for archeological objects [36–39]. These phenomena are the main causes of corrosion observed for G_D as confirmed by the results shown in fig. 2(d).

Objects A and C show similarity regarding not only their appearance, surface ornamentation and dating (XIX century), but also their composition, which, however, is not necessarily substantive information, as shown by Barnet

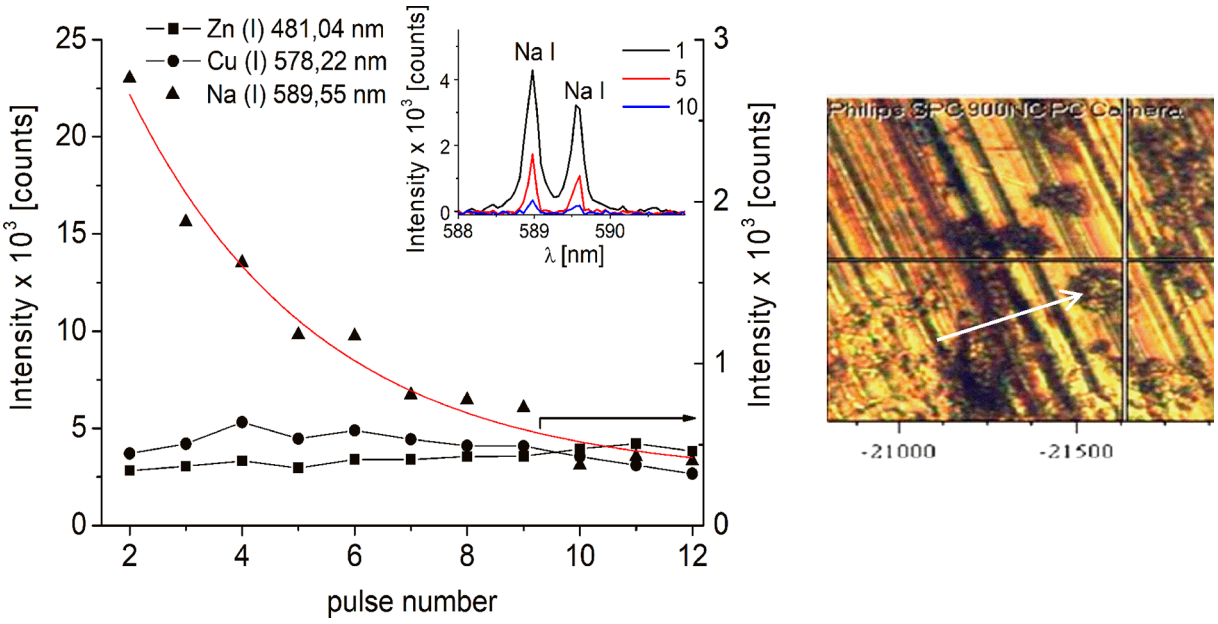

Fig. 4. Change in peak intensity of the emission lines of Zn, Cu, and Na observed in LIBS spectra as a result of penetration beyond the surface of object A after a series of successive laser pulses. The inset shows profiles of the Na peak corresponding to the 2nd, 5th and 10th laser pulse. The image on the right shows an example of the surface perforation after the measurement with a crater size of about 120 μm.

and Dandridge [28] who discussed the authenticity of medieval style aquamanilia produced in the nineteenth and early twentieth centuries. XRF spectra corresponding to objects A and C shown in fig. 3(a) reveals the presence of the same major alloy components (Cu and Zn) together with minor elements. However, peaks which could be ascribed to surface contamination and painted remains of the decoration (see inset in fig. 3(a)) were not observed. It should be mentioned that a direct comparison of the peak intensities observed for Zn and minor elements (Sn, Pb, Ni, and Fe) in spectra A and C can be misleading because of the use of different instruments XRF_I and XRF_{II} [7].

Complementary measurements with the use of micro-invasive LIBS supported the XRF results through similarities found in the spectra recorded for A and C in comparison with other objects studied. This can be seen after comparison of the XRF and LIBS spectra in fig. 3(a) and (b). The peaks observed in the LIB spectra can be ascribed to elements Zn (468.0; 472.2; 481.0 nm), Cu (510.5; 515.4; 521.82 nm), Sn (326.2 nm), Pb (357.4; 368.4 nm), and to admixtures (or traces) of Ag, Ni, and Fe typical for some copper ores (*e.g.*, chalcopyrite, $CuFeS_2$) [36]. The latter ones are important markers for studies on the origin, production technology, and trade routes of the alloys. Peaks of sulphur are not observed in the LIB spectra, and therefore, the presence of sulphides, characteristic of the patina, can be excluded confirming that the iron content is related to copper ores used for alloy production.

Bands corresponding to the major (Cu, Zn) and minor (Sn, Ag, Ni) alloy components can be observed with minimal overlap (Fe peak at 334.6 nm is not marked for clarity) in the 321–337.5 nm spectral range (see inset in fig. 3(b)) [40].

Compared to XRF, the LIBS spectra show additionally relatively strong peaks of Na at 589.6 nm (objects A, C) and Ca at 616.2 nm (A) which originate most likely from surface contamination as discussed elsewhere [36,39,41]. This was confirmed by stratigraphic measurements where spectra were acquired while penetrating below the surface by performing a series of consecutive laser pulses. A series of 15 laser pulses results in a crater with a width of approximately 120 μm and a depth of about 16–20 μm (fig. 4(a)), in agreement with effects reported by other authors [10]. The pulse-number-dependent peak intensities corresponding to major components of the alloy (Cu and Zn) as well as to Na are plotted in fig. 4(b). The inset shows a decrease in Na band intensity corresponding to the 2nd, 5th, and 10th laser pulse. The nearly constant intensities of the Zn and Cu peaks with increasing laser pulse number are accompanied by an instantaneous marked decay observed for Na. This progression indicates that this element belongs to the successively removed contamination layer.

The material composition observed for objects A, C, G, D, and E (not shown) revealed similar elemental content and indicated the use of ternary or quaternary copper alloys. The major elements identified were Cu and Zn, while Sn and Zn were identified as minor elements. Moreover, the spectra showed trace amounts of Fe, Ni, Si, and Ag. In contrast, XRF spectra of object F showed dominant bands of Sn and Pb and absence of Cu. Strong Sn and Pb lines were also identified in the LIB spectrum. These results together with the grayish surface color and higher mass of object F, compared to B and C of similar dimensions, confirm the presence of a Sn-Pb alloy.

Table 2. Alloy compositions of *aquamanilia* obtained from XRF measurements.

		Zn (%)	Cu (%)	Sn (%)	Pb (%)	Other (%)	Minor and/or trace elements	Material
A	XRF_I	22.9 ± 4.1	69.8 ± 5.0	4.4 ± 0.6	2.0 ± 0.4	$\sim 0.9\%$	Fe, Ni, Ag	Brass
A_D		40.0 ± 7.2	44.0 ± 3.5	1.9 ± 0.3	2.6 ± 0.5	$\sim 0.8\%$		
B[(a)]	XRF	5.0	$\sim 81\%$	7.0	5.4	Fe 1.1; Ni 0.1 As 0.2; Ag 0.2 Sb 0.04 Cd 0.02 Au 0.005	Bi	Bronze
C	XRF_{II}	20.2 ± 4.5	75.4 ± 2.5	0.6 ± 0.1	0.6 ± 0.1	3.2 ± 0.8	Fe, Ba, Na	Brass
D	XRF_{II}	17.9 ± 4.5	78.4 ± 2.5	0.5 ± 0.1	1.9 ± 0.1	1.3 ± 0.1	Fe, Ba, Na	Brass
E	XRF_{II}	19.7 ± 4.5	77.8 ± 2.5	–	1.9 ± 0.1	0.6 ± 0.4	Fe, Ba, Na	Brass
F[(b)]	XRF_T	–	4.0 ± 2.5	67.7 ± 11.5	22.9 ± 2.3	5.4 ± 0.4	S 3.4; Sb 1.2 Fe 0.5	Tin-Lead Alloy
G	XRF_I	22.0 ± 4.0	75.0 ± 6.0	4.6 ± 0.6	0.9 ± 0.2	~ 0.2	Ni, Fe, Ag	Brass
G_D	XRF_I	15.3 ± 7	76.9 ± 2.4	3.3 ± 1.3	1.8 ± 0.3	$\sim 1.9\%$	Ni, Fe, Ag (S?)	Brass, Corrosion traces

[(a)] Data from [23].
[(b)] Measured with the XRF_T analyzer (S1 Titan).

4.2 Quantitative analysis

The quantitative analysis of the alloys was conducted using the instruments described above: XRF_I, XRF_{II}, and LIBS. Spectral data were derived from deconvolution of the background-subtracted peaks using the WinQXAS package. The calibration results for Cu, Zn, Sn, and Pb are shown as supplementary material in fig. S1(a) (ESM). For estimation of the XRF_I calibration uncertainty, five measurements were conducted on each standard and the data were averaged. Values of the mean relative standard deviation (RSD_m) between the measured and nominal contents, $(C_m - C_n)/C_n$, were equal to 6.0, 5.0, 1.0 and 0.5% for Cu, Zn, Sn, and Pb, respectively. The error of prediction calculated for Cu, Zn, Sn, and Pb was 1.5, 0.2, 0.8, and 0.4, respectively.

In the case of XRF_{II}, RSD_m values of 2.5, 4.5, and 0.1% were obtained for Cu, Zn, and Pb, respectively. These values were determined from a direct comparison of the count rates measured for the standards and a calibration procedure that has been described in detail elsewhere [42]. The net peak areas (NPA) were used to calculate the intensity ratio of the main elements (NPA_{Cu}/NPA_{Zn}) with respect to the concentration ratio (C_{Cu}/C_{Zn}) reported for the standards. The calibration curve obtained was used for determination of the Cu/Zn concentration ratio of the investigated objects. In a similar way, the Zn concentration was obtained from the NPA_{Zn}/NPA_{Pb} or NPA_{Zn}/NPA_{Sn} ratios. The choice of Pb *versus* Sn, or vice versa, was based on the higher relative area obtained after comparing the values obtained for these two elements. The unknown values of C_{Pb} or C_{Sn} were determined from the calibration curves obtained for these two elements in which the areas (NPA_{Pb} or NPA_{Sn}) were plotted against the standard concentrations (C_{Pb} or C_{Sn}). Subsequently, the unknown concentration of Cu was calculated using a modified version of the equation given in [42]:

$$C_{Cu} = M \times C_{Cu/Zn} \times \left(1 + C_{Cu/Zn} + \frac{1}{C_{Zn/X}}\right)^{-1}, \quad (1)$$

where M is the sum of concentrations of the main elements $M = C_{Cu} + C_{Zn} + C_X$, with C_X being the concentration of Pb or Sn depending on the object, and $C_{Cu/Zn}$, $C_{Zn/X}$, the concentration ratios of the corresponding elements. The total concentration of trace elements was assumed to be approximately 1% which resulted in $M = 99\%$. The calibration results of XRF_{II} are given in fig. S1(b) (ESM).

For calibration of the LIBS instrument the most relevant spectral lines of Cu (510.56 nm), Zn (481.04 nm) and Sn (326.35 nm), showing highest signal-to-noise ratio, were selected in order to minimize the effect of spectral interference and self-absorption [43]. Because of the relatively large signal fluctuations, the concentrations of the major components (Zn and Sn) were obtained from peak intensity values related to Cu (fig. S1(c), ESM).

The alloy compositions of the *aquamanilia* are reported in tables 2, 3, and S2 (ESM). For objects A, C, and G, the contents of Zn and Cu varied in the ranges 20–23% and 70–75%, respectively. The Zn content in the defect area A_D ($40 \pm 7\%$) was nearly two times higher than the one obtained for the original alloy A. This result indicates that the defect area of this *aquamanile* consists of a modern brass. LIBS stratigraphy measurements allowed to study the effects caused by surface contamination. Object G contained areas showing a Cu content of about 75% in the surface layer. This was relatively lower when compared to the values obtained for the prevailing surface area.

Table 3. Estimated concentration of the main alloy elements of *aquamanilia* A, C, D, and E obtained from LIBS measurements.

Object	Zn (%)	Cu (%)	Sn+Pb (%)	Minor and trace elements	Material
A	17.0 ± 2.2	74.0 ± 16.3	8.5 ± 2.1		Ternary or quaternary brass alloy
C	22.1 ± 4.9	70.7 ± 15.5	7.2 ± 1.2	Fe, Ag, Ni Ca, Ba, Na	
D	17.5 ± 3.8	74.5 ± 16.4	8.1 ± 1.3		
E	15.2 ± 3.3	76.8 ± 16.9	8.1 ± 1.3		

These observations were ascribed to the prolonged exposure of the object to the corrosive seawater environment. Objects A and G contained a relatively higher amount of Zn and together with D and E can be classified as ternary or quaternary Cu alloys based on the content of minor elements Sn and Pb.

A comprehensive discussion on the variations in crystallographic properties of brass alloys due to the addition of different percentages of Zn can be found in the dissertation of Bacon [44]. In her work, the author describes the two principal methods of manufacturing brass. The earlier method was the cementation process, which consists of diffusing two solids together, while the later one is direct alloying of Cu and Zn metal. Furthermore, the author made reference to over forty standard compositions for brass with zinc contents ranging from 5% to 40%. In general, ancient and medieval brasses have a maximum Zn content of 28–30%, while modern brasses have a relatively higher Zn content (30%–40%). The higher Zn content of modern brasses is associated with production through the direct method, as opposed to earlier brasses, which were typically made by the cementation process [45]. After comparing the brass objects analyzed within the current study (A, C, D, E, G), it can be seen that the Zn contents were in the range 18–23%. According to Craddock [45], low Zn contents are typical of medieval and post-medieval European brasses. A higher Zn content ($> 33\%$) is expected for objects manufactured from the XVI century to the present day. Of the objects evaluated, only E is dated to the end of the XV century, while the remaining four were dated back to between the XIX and the XX centuries. Although a higher Zn content is expected for the latter ones, Craddock indicates that brasses produced from the ancient to post-medieval periods are suspicious if they contain more than 28%–33% of Zn. This was not the case for any of the original brass surfaces evaluated in the current study. However, as indicated above, a higher Zn content obtained for a repaired area of object A provides evidence of the use of a modern brass for the restoration. In contrast, the material composition of the reference object B is characteristic for bronze alloys [29]. The XRF measurements for this *aquamanile* were performed by Werner for object documentation in 1972 and are in agreement with data published by himself in 1980, and were confirmed by GNN —courtesy of Dr. R. Schuerer, recently.

In the case of the object G a relatively higher amount of Sn (3.9%) seems intentional and aimed at making an alloy of improved properties [36]. This follows from the work of Campanella *et al.* [40] who observed that a Sn content $> 1\%$ in Cu alloys acts as an inhibiting agent reducing the tendency toward dezincification. The larger deviations observed for the Cu concentration estimated for object E are very likely due to a higher number of surface irregularities relative to other objects. In the case of LIBS, the Cu concentrations obtained from averaged spectra (due to signal fluctuation) are in satisfactory agreement with values estimated by subtracting the concentrations of Zn and other elements from the total content of 100%. This confirms the advantage of the performed averaging in case of the sampled surface (underside of foot) and in view of the commonly accepted opinion that qualitative LIBS analysis is reliable if the object has a homogeneous surface.

The alloys' composition together with the measurement dispersion expressed as the standard deviation indicate that the uncertainty of LIBS measurements is generally higher than that of XRF, *i.e.* up to 17% *versus* 5% for Cu. The discrepancy between the XRF and LIBS data observed for object A originates mainly from inhomogeneity of the alloy and surface effects.

A common assumption made when interpreting XRF data of metallic cultural heritage objects is to assume that they are homogeneous throughout their entire surface as well as in the bulk. The depth of penetration of X-rays is influenced by a number of factors including: the density of the material, the fluorescence energy of the chemical elements in the object, and the energy of the X-ray beam [46]. The photons emitted by the X-ray source are usually absorbed by the object's surface, limiting the information range to about 10–100 micrometers [47]. Moreover, the corrosion layer may exhibit different thicknesses throughout a single object limiting the quantitative analysis since XRF spectra will contain information not only about the metal alloy, but also about the corrosion products present. Acknowledging these limitations and understanding their consequences in the analysis is important when investigating museum objects as these deviations can significantly increase the uncertainty of the results. Several measures can be taken to minimize the error if the surface of the object is highly corroded. For example, cross section analysis may be conducted to determine the thickness of the corrosion layer, performing XRF analysis after removal of corrosion on clean metallic surfaces, and increasing the number of analysis spots to have better statistical representativeness of the data. A more recent approach is to study microsamples extracted from objects using nano-invasive focused ion beam-field emission scanning electron microscopy-X-ray microanalysis (FIB-FESEM-EDX) [48], in which only a few nanograms of matter are lost during the analysis. This complementary technique is very appropriate to study the subsurface region of an object, which has not experienced any modifications due to undocumented cleaning methods and/or conservation treatments.

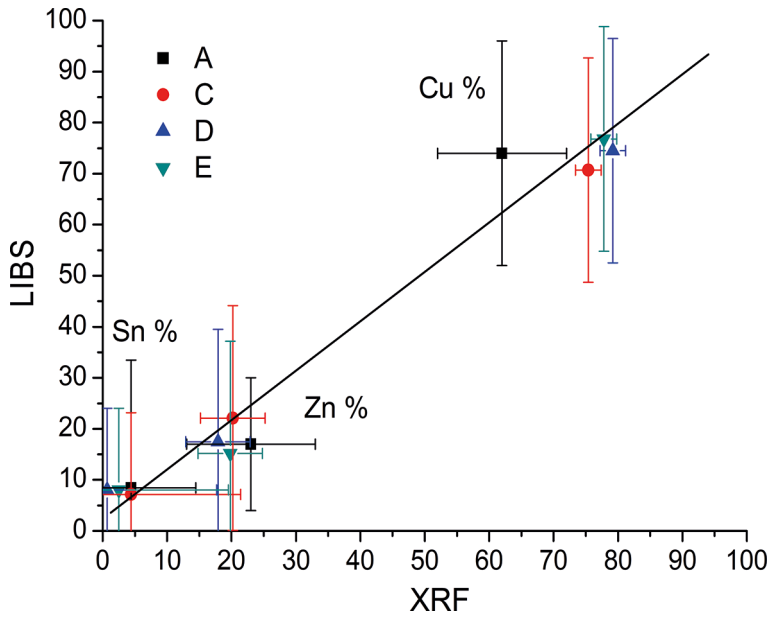

Fig. 5. Summary of the correlation between LIBS and XRF quantitative analysis for Cu, Sn and Zn obtained by averaging the net peak areas from a series of spectra collected on inconspicuous areas of objects A, C, D, and E.

The accuracy level obtained for LIBS measurements seems better than acceptable when sampling conditions and phenomena affecting the recorded signal are taken into account [31,49]. The relatively higher values of Sn obtained by LIBS with respect to XRF for objects A, C, D, and E point towards systematic errors originating from calibration. The results and their corresponding standard deviations are summarized in fig. 5. The general correlation between XRF and LIBS data observed for objects A, C, D, and E is satisfactory and is in agreement with the results reported for historical alloys by other authors [50–52]. A closer inspection of the XRF/LIBS correlation observed separately for the alloy elements Cu, Zn and Sn revealed marked differences between the corresponding values of the standard deviation (fig. S2, ESM). This supports the previous conclusion and is in agreement with the characteristic signal fluctuation of consecutive measurements, which vary according to the surface and local geometry. The dispersion of the data (fig. S3, ESM) indicates that measurements performed on real objects *in situ* require averaging of a sufficient number of points in order to obtain reliable results. Another approach for the verification of the data could be the use of another instrument (table S1, ESM). It can be seen that the discussed effect is more noticeable in LIBS relative to XRF due to inevitable intensity fluctuations of the laser beam intensity, absorbed pulse energy, and plasma interaction.

4.3 Comparison with reference objects

To better understand the scattering of the measured values and to validate the XRF results, the data collected for the *aquamanilia* were contrasted with results obtained for a reference group of historical brass objects selected by art historians from the collection of MNG and fabricated between XVI–XVIII centuries: three candlesticks (R1, R2, R3), and a water tap (R4). To do so, the entire collection of XRF results has been processed by means of Principal Component Analysis (PCA), which is a useful tool in reducing problems associated with the analysis of heterogeneous heritage substances [53]. This method provides a compressed subspace of a few principal components, which allow resolving and separating clusters of similar data, while discriminating outliers. The procedure can be implemented prior to performing a detailed quantitative analysis, too [12,53]. For the PCA performed here a total of 30 XRF spectra were acquired from different locations on each *aquamanile* and on the reference objects R1-R4. The results are presented as the relation between PC1 and PC2 representing the most dominant spectral features (fig. 6(a)). Each data point represents one spectrum and the spectral similarities are directly related to the spacing between the data points. Singular points distinctly separated from corresponding groups and marked by circles/ovals can be treated as outliers.

The correlation between the *aquamanile* A and the candlestick R1, dated back to the XVIII century, indicates a similar alloy composition for these two objects. This result together with the datum "1744" stamped on A support the hypothesis that these two objects were produced in a similar time period, providing additional information about the historical value of A representing a replica of a medieval aquamanile. Most of the scattered points belonging to A_D are well separated from those corresponding to A, which is in accord with the difference detected for the alloys used in A_D and A. While PC2 values observed for A_D are higher than those of A_S, they do not differ much for other objects.

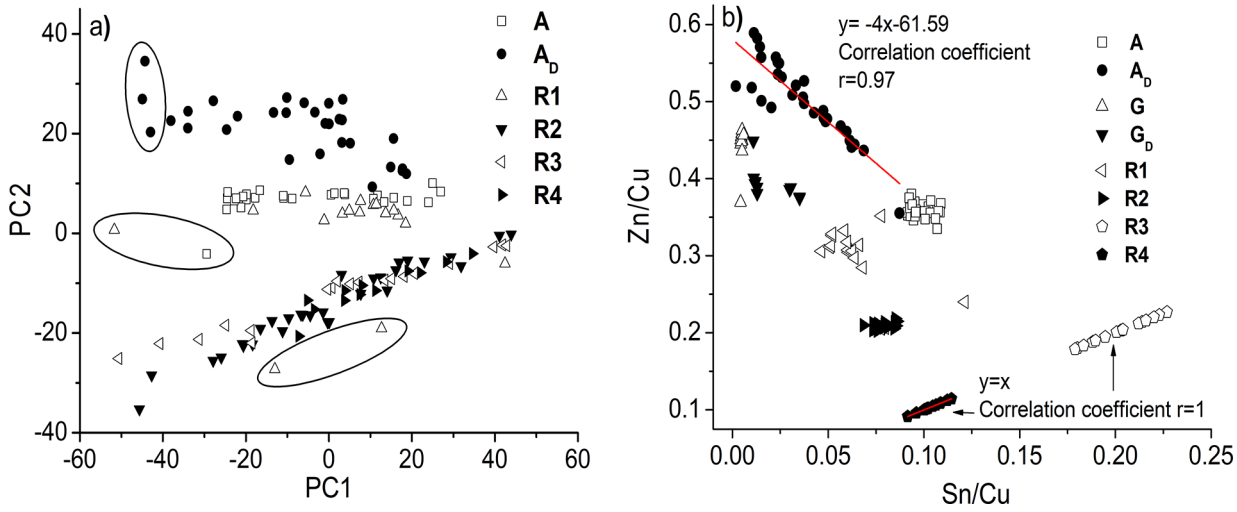

Fig. 6. Summary of results of the PCA analysis: (a) data extracted from XRF spectra of A recorded from original surface (A) and defect areas (A_D) together with those obtained for the brass reference objects; data points of low relevance are enclosed by ovals, (b) Data as in (a) complemented with those of G and G_D shown as a plot of the Zn/Cu *versus* Sn/Cu ratio.

The corresponding PC2 data show differences, not only for A_D, but also for A and the four candlesticks. It can be assumed that PC2 and PC1 correlate with the ratios of Zn/Cu and with the remaining elements, mainly Sn, Pb, related to the Cu+Zn content. This can be better illustrated after evaluating the results of PCA analysis for the alloy compositions. XRF data corresponding to net peak areas of Zn and Sn related to Cu are shown for all investigated objects in fig. 6(b). The eight separated data groups show a relatively high Zn content for historical alloys (A_D, R1-R4) and a markedly higher one for the defect area A_D. In addition, the closer distance observed between A and R1 confirms their compositional similarity. The separation of dispersed A_D data and the relative positions of G and G_D offer evidence about the repair of the *aquamanile* A and the dezincification experienced by object G. Data points that form straight lines indicate local variations of the overall XRF signal.

5 Conclusions

The material composition of a group of *aquamanilia* housed in museums in Kraków and Gdańsk were investigated in order to support studies on their authentication and dating. The results were obtained by performing complementary XRF and LIBS measurements *in situ* with the use of portable instruments. It has been shown that, with one exception, the objects under question were cast using ternary and quaternary Cu-alloys revealing consistently a relatively large Zn content up to 23%, and contents of Sn and Pb in the range of 0.7–4.4% and up to 0.7%, respectively. The XRF and LIBS spectra revealed, besides Cu, the presence of strong bands ascribed to Zn, Sn, Pb and also weaker ones associated with admixtures and impurities such as Ag, Fe, and Ni, and surface contamination was detected by means of LIBS stratigraphy, too. The obtained results show consistence with: i) evolution history of Cu-alloy compositions and related production technologies (see, *e.g.*, Craddock [45]); ii) results of extensive studies devoted to aquamanilia reported by Barnet and Dandridge [28]; and iii) known art historical data. This implies that the brass figure (with contemporary repair showing 44% Zn) of a lion from the National Museum in Gdańsk dates back to the XVIII century and represents a replica of a medieval aquamanilia. Another of the investigated figures (small dragon), locally showed a lower Cu content ($\sim$ 75%) when compared with the prevailing surfaces and in view of the above-mentioned literature data, the observed effect was ascribed to prolonged exposure of the object to the corrosive seawater environment.

The differences observed between the quantitative data obtained using the two aforementioned techniques were ascribed to various effects including the surface patina, contamination, surface irregularities, and material inhomogeneity. These have been typically identified as sources of error to be considered when performing quantitative analysis of cultural heritage objects. The standard deviations observed in the analysis of certified standards used for instrument calibration contributed to systematic errors during quantification. For all these reasons, while confirming the usefulness of the complementary XRF and LIBS analysis of the metallic historical objects, the authors understand that comparison of the absolute elemental concentrations provide not always sufficiently reliable results. A supporting measure which summarizes the analysis and compares the composition of the objects, *e.g.*, using statistical methods is recommended since similarities and differences within a group of objects can be better understood and described. Further research includes adding appropriate certified standards and analyzing a larger group of representative objects in order to improve the instrument calibration and ensure a higher statistical significance of the results, respectively.

The authors are grateful to Dr. R. Schürer for the data on the medieval aquamanile and to Mrs. A. Fietkiewicz and Dr. Ł. Bratasz for providing part of the objects. P. Świt and P. Jóźwiak are acknowledged for processing the XRF_{II} data and photographic documentation, respectively. Dr. W. Skrzeczanowski is acknowledged for discussion of the LIBS results. This research was funded by the Ministry of Science and Higher Education of Poland (MNiSW) via grant 60/E-87/S/2012.

References

1. E. Pernicka, *Archaeometallurgy in Global Perspective*, edited by B. Roberts, C. Thornton (Springer, New York, 2014).
2. M.F. Guerra *et al.*, *Radiation in Art and Archaeology*, edited by D.C. Creagh, D.A. Bradley (Elsevier, New York, 2000).
3. I. De Ryck, A. Adriaens, F. Adams, Archaeometry **45**, 579 (2003).
4. P. Dillmann, D. Watkinson, E. Angelini, A. Adriaens, *Corrosion and Conservation of Cultural Heritage Metallic Artefacts* (Woodhead, Cambridge, UK, 2013).
5. M.C. Bernard, S. Joiret, Electrochim. Acta **54**, 5199 (2009).
6. Ł. Selwyn, *Metals and Corrosion: A Handbook for the Conservation Professional* (Canadian Conservation Institute, Ottawa, CA, 2004).
7. A. Arafat, M. Na'es, V. Kantarelou, N. Haddad, A. Giakoumaki, V. Argyropoulos, D. Anglos, A.-G. Karydas, J. Cult. Herit. **14**, 261 (2013).
8. L. Ciupiński, E. Fortuna-Zaleśna, H. Garbacz, A. Koss, K.J. Kurzydłowski, J. Marczak, J. Mróz, T. Onyszczuk, A. Rycyk, A. Sarzyński, W. Skrzeczanowski, M. Strzelec, A. Zatorska, G.Z. Żukowska, Sensors **10**, 4926 (2010).
9. R. Cesareo, M. Ferretti, G.E. Gigante, G. Guida, P. Moioli, S. Ridolfi, C. Roldán Garcia, X-Ray Spectrom. **36**, 167 (2007).
10. A. Nevin, G. Spoto, D. Anglos, Appl. Phys. A **106**, 339 (2012).
11. I. Żmuda-Trzebiatowska, A. Fietkiewicz, G. Śliwiński, Solid State Phenom. **183**, 233 (2011).
12. A. Iwulska, R. Jendrzejewski, M. Sawczak, I. Żmuda-Trzebiatowska, G. Śliwiński, in *Proceedings of the Lasers in the Conservation of Artworks VIII, 2010*, edited by R. Radvan, J.F. Asmus, M. Castillejo, P. Pouli, A. Nevin (CRC, Boca Raton, 2010).
13. J. Agresti, A. Mencaglia, S. Siano, Anal. Bioanal. Chem. **395**, 2255 (2009).
14. L. Caneve, F. Colao, R. Fantoni, V. Spizzichino, Appl. Phys. A **85**, 151 (2006).
15. A.N. Shugar, J.L. Mass, *Handheld XRF for Art and Archaeology* (Leuven University, Leuven, BE, 2013).
16. E. Frahm, R.C.P. Doonan, J. Archaeol. Sci. **40**, 1425 (2013).
17. S. Klein, J. Hildenhagen, K. Dickmann, T. Stratoudaki, V. Zafiropulos, J. Cult. Herit. **1**, 287 (2000).
18. M. Simileanu, Rom. Rep. Phys. **68**, 203 (2016).
19. M. Castillejo, M. Martín, D. Silva, T. Stratoudaki, D. Anglos, L. Burgio, R.J.H. Clark, J. Cult. Herit. **1**, S297 (2000).
20. K. Ochocińska, M. Sawczak, M. Martin, J. Bredal-Jørgensen, A. Kamińska, G. Śliwiński, Rad. Phys. Chem. **68**, 227 (2003).
21. V. Spizzichino, R. Fantoni, Spectrochim. Acta B **99**, 201 (2014).
22. D. Anglos, V. Detalle, S. Musazzi, U. Perini (Editors), *Laser Induced Breakdown Spectroscopy* (Springer, Berlin, Heidelberg, 2014).
23. E.H. Lehmann, P. Vontobel, E. Deschler-Erb, M. Soares, Nucl. Instrum. Methods Phys. Res. A **542**, 68 (2005).
24. M.P. Morigi, F. Casali, M. Bettuzi, R. Brancaccio, V. D'Errico, Appl. Phys. A Mater. **100**, 653 (2010).
25. G. Sarah, B. Gratuze, J.N. Barrandon, J. Anal. At. Spectrom. **22**, 1163 (2007).
26. M. Dowsett, A. Adriaens, Nucl. Instrum. Methods Phys. Res. B **226**, 38 (2004).
27. E. Tognoni, V. Palleschi, M. Corsi, G. Cristoforetti, N. Omenneto, I. Gornushkin, B.W. Smith, J.D. Winefordner, *Laser-Induced Breakdown Spectroscopy, Fundamental and Applications*, edited by A.W. Miziolek, V. Palleschi, I. Schechter (Cambridge University, Cambridge, UK, 2006).
28. P. Barnet, P. Dandridge (Editors), *Lions, Dragons, and Other Beasts: Aquamanila of the Middle Ages, Vessels for Church and Fid* (Yale University Press, New Haven, CT, 2006).
29. O. Werner, *Zusammensetzung neuzeitlicher Nachgüsse und Fälschungen mittelalterlicher Messinge und Bronzen* (Archäometrie, Berliner Beitr. 5, 11 1980).
30. O.v. Falke, E. Meyer, *Romanische Leuchter und Gefäße Gießgefäße der Gotik* (Deutsche Verlag für Kunstwissenschaft, Berlin, 1937).
31. H.P. Lockner, Kunst Antiq. **5**, 28 (1981).
32. Metropolitan Museum of Art (2018) `http://www.metmuseum.org/`.
33. M. McAllister, Western Australia, Bull. Australasian Inst. Mar. Archaeol. **36**, 36 (2012).
34. G. Pantazopoulos, A. Vazdirvanidis, Mater. Sci. Eng. **55**, 012015 (2014).
35. H. Sugawara, H. Ebiko, Corrosion Sci. **7**, 513 (1967).
36. D.A. Scott, *Conservation, Paul Getty Ancient & Historic Metals: Conservation and Scientific Research* (Conservation Institute, Malibou California, USA, 2002).
37. K.R. Trethewey, I. Pinwill, Surf. Coat. Technol. **30**, 289 (1987).
38. M.M. Megahed, Int. J. Conser. Sci. **5**, 161 (2014).

39. F. Schweitzer, *Proceedings of Ancient and Historic Metals: Conservation and Scientific Research Symposium organized by the Paul Getty Museum, Los Angeles, 1991*, edited by D.A. Scott, J. Podany, B.B. Considine (J. Paul Getty Museum, California, 1994).
40. L. Campanella, O. Colacichi Alessandri, M. Ferretti, S.H. Plattner, Corros. Sci. **51**, 2183 (2009).
41. M. Morcillo, E. Almeida, M. Marrocos, B. Rosales, Corrosion **57**, 967 (2001).
42. J.M. del Hoyo-Melendez, P. Świt, M. Matosz, M. Woźniak, A. Klisińska-Kopacz, Ł. Bratasz, Nucl. Instrum. Methods Phys. Res. B **349**, 6 (2015).
43. National Institute of Standards and Technology (2018) `http://physics.nist.gov/asd`.
44. A.L. Bacon, *A Technical Study of the Alloy Compositions of 'Brass' Wind Musical Instruments (1651-1867) Utilizing Non-Destructive X-ray Fluorescence*, PhD Dissertation University College London (ProQuest, Ann Arbor, US, 2003).
45. P. Craddock, *Scientific Investigation of Copies, Fakes and Forgeries* (Elsevier, New York, US, 2009).
46. K.H.A. Janssens, F.C.V. Adams, A. Rindby, *Microscopic X-ray Fluorescence Analysis* (Wiley, New York, US, 2000).
47. B. Constantinescu, R. Bugoi, E. Oberländer-Târnoveanu, K. Pârvan, Rom. Rep. Phys. **57**, 1021 (2005).
48. M.T. Doménech-Carbó, F. Di Turo, N. Montoya, A.F. Catalli, A. Doménech-Carbó, C. De Vito, Sci. Rep. **8**, 1 (2018).
49. R. Jenkins, X-Ray Fluorescence Spectrometry, 2nd ed. (John Wiley and Sons, New York, NY, 1999).
50. M. Ferretti, C. Cristoforetti, S. Legnaioli, V. Palleschi, A. Salvetti, E. Tognoni, E. Console, P. Palaia, Spectrochim. Acta B **62**, 1512 (2007).
51. L. Pardini, A. El Hassan, M. Ferretti, A. Foresta, S. Legnaioli, G. Lorenzetti, E. Nebbia, F. Catalli, M.A. Harith, D. Diaz Pace, F. Anabitarte Garcia, M. Scuotto, V. Palleschi, Spectrochim. Acta B **74-75**, 156 (2012).
52. V. Lazic, M. Vadrucci, R. Fantoni, M. Chiari, A. Mazzinghi, A. Gorghinian, Spectrochim. Acta B **149**, 1 (2018).
53. R. Gaudiuso, M. Dell'Aglio, O. De Pascale, G.S. Senesi, A. De Giacomo, Sensors **10**, 7434 (2010).